# Supplementary Information

## Decoupling Layer Metal-Organic-Frameworks via Ligand Regulation to Achieving Ultra-Thin Carbon Nanosheets for Oxygen Reduction Electrocatalysis

*Zeming Tang, Guiqiang Cao, Cheng Jiang, Jianping He, Adeline Loh, Zhongxu Wang, Jingxiang Zhao, Xiaohong Li,* Qingxue Lai,* Yanyu Liang**

### Supplementary Figures

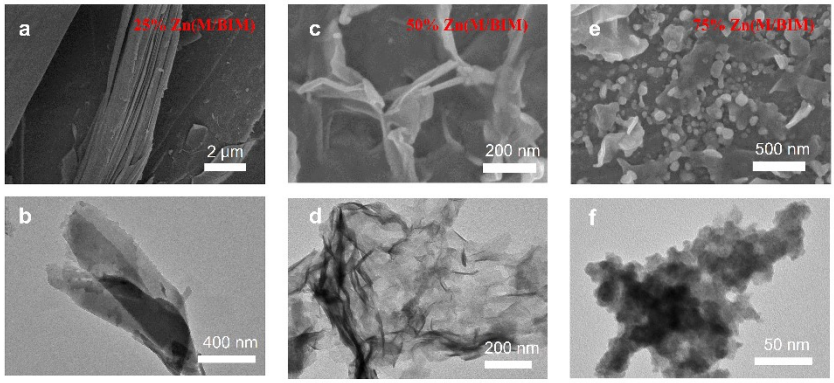


Figure S1. SEM and TEM images of (a,b) 25% Zn(M/BIM) MOFs; (c,d) 25% Zn(M/BIM) MOFs and (e,f) 75% Zn(M/BIM) MOFs

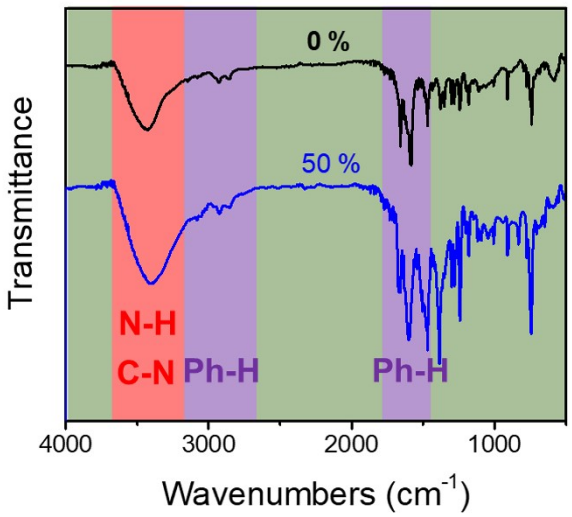


Figure S2. FT-IR pattern of Zn(BIM) and 50% Zn(M/BIM)

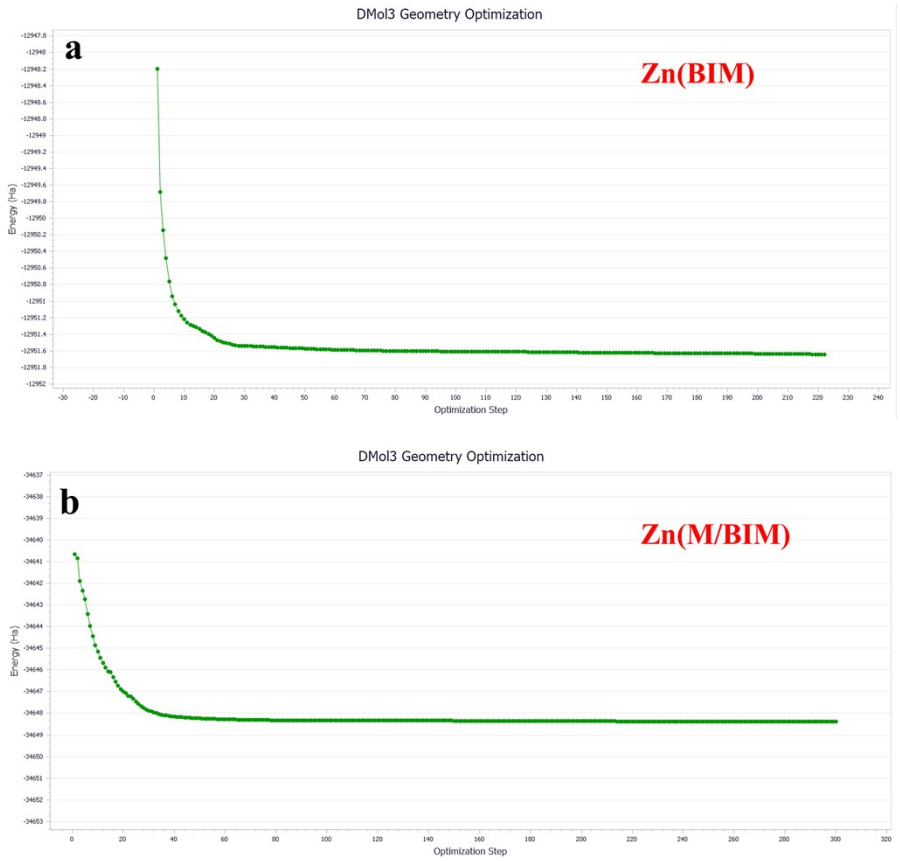


Figure S3. The raw data of optimization step of (a) Zn(BIM) MOFs and (b) Zn(M/BIM) MOFs. Self-consistent field (SCF) convergence precision is set at $10^{-4}$.

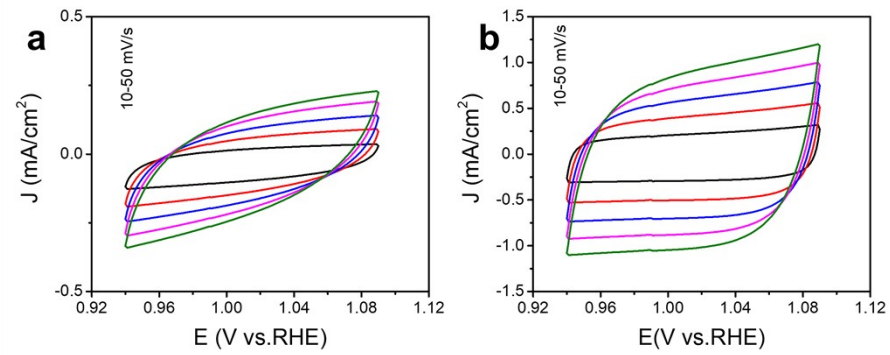


Figure S4. (a,b) CV curves of N-C(BIM) and N-C(M/BIM).

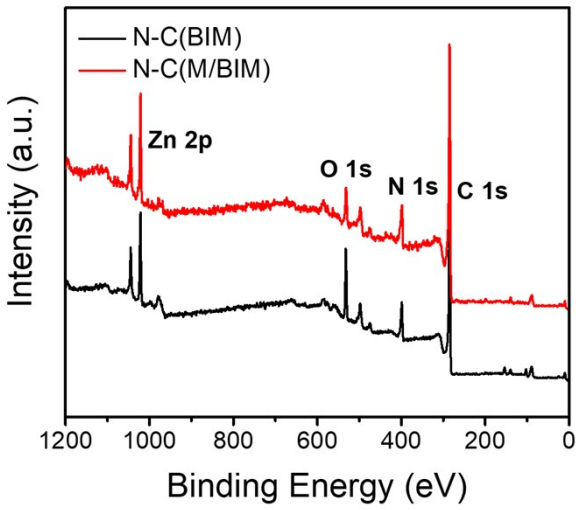


Figure S5. XPS spectra of N-C(BIM) and N-C(M/BIM).

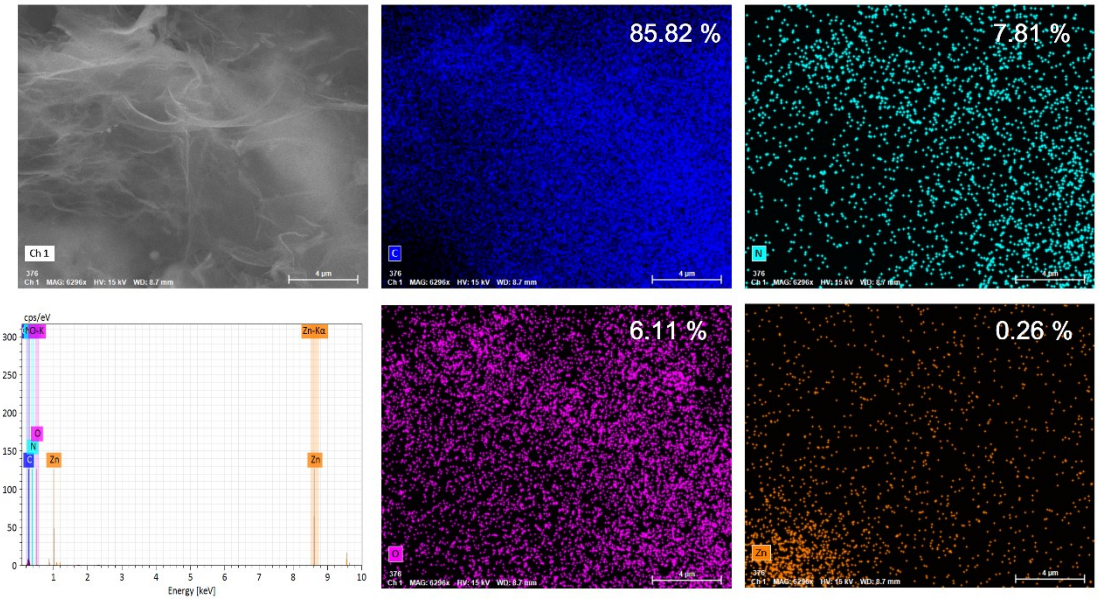


Figure S6. Energy dispersive spectrometer (EDS) spectra and elemental mapping images of UT-N@N-C(M/BIM).

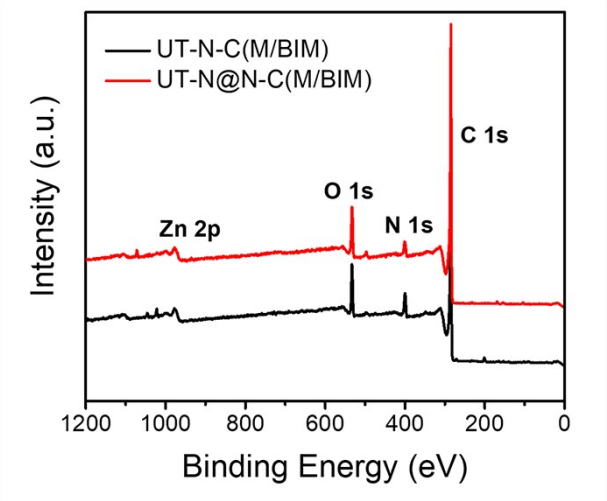


Figure S7. XPS spectra of UT- N-C(M/BIM) and UT-N@N-C(M/BIM)

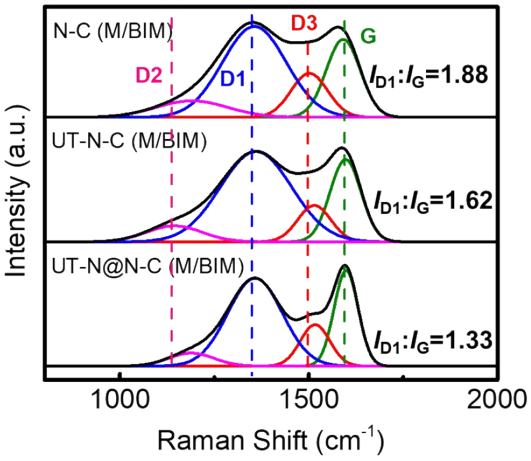


Figure S8. Raman spectra of N-C (M/BIM), UT-N-C (M/BIM) and UT-N@N-C (M/BIM).

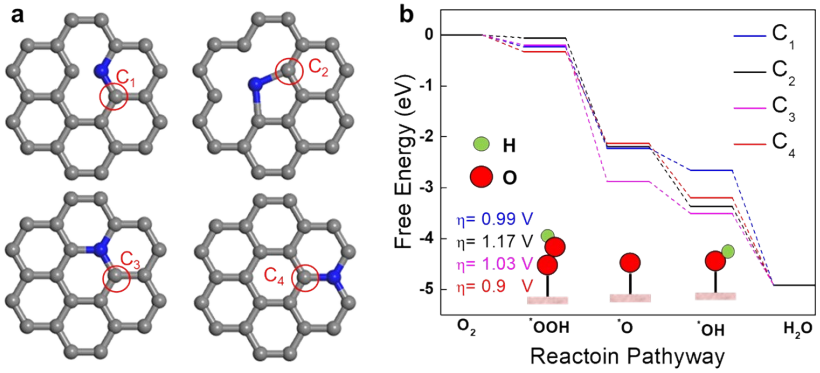


Figure S9. (a) DFT-optimized carbon sites with different N-doping models; (b) ORR free energy diagrams calculated for the four C sites.

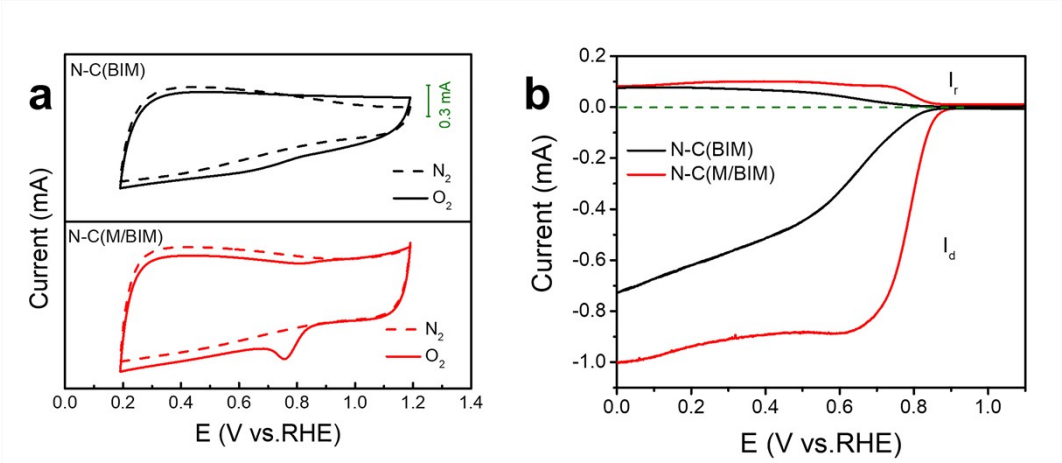


Figure S10. (a) CV curves of N-C(BIM) and N-C(M/BIM) on glassy carbon electrodes in $O_2$-saturated (solid line) and $N_2$-saturated (dash line) 0.1 M KOH; (b) Rotating ring-disk electrode voltammograms recorded with N-C(BIM) and N-C(M/BIM) in $O_2$-saturated 0.1 M KOH at 1,600 r.p.m.

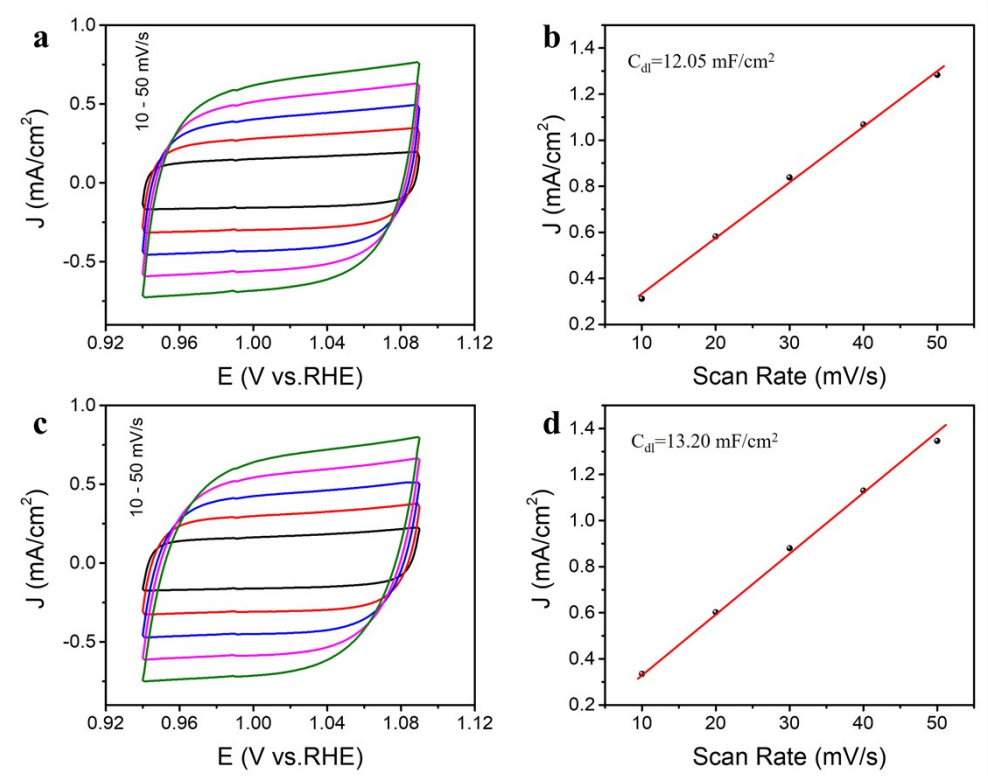


Figure S11. (a,c) CV curves of UT-N-C(M/BIM) and UT-N@N-C(M/BIM); (b,d)The capacitive current measured at 1.00 V(vs.RHE) plotted as a function of scan rate of UT-N-C(M/BIM) and UT-N@N-C(M/BIM).

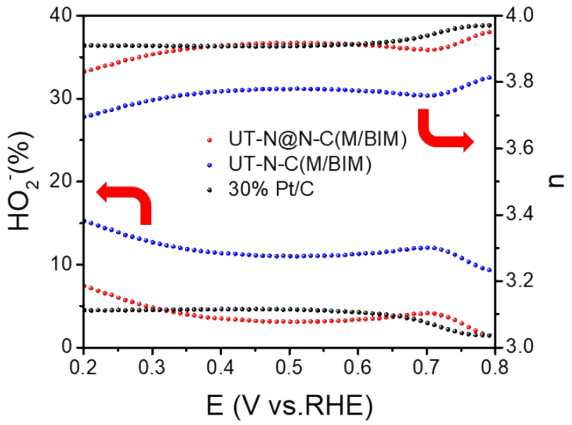


Figure S12. Percentage of peroxide (lower line) and the electron transfer number (n) (upper line) of UT-N-C(M/BIM) and UT-N@N-C(M/BIM).

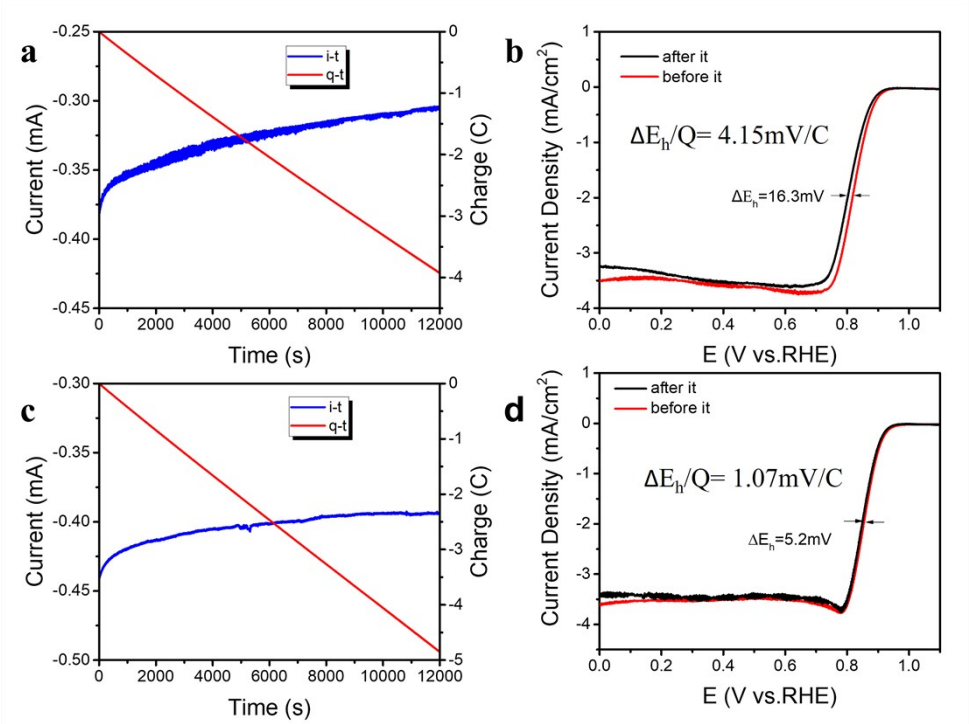


Figure S13. (a,c)I-t curves and transfer charge of UT-N-C(M/BIM) and UT-N@N-C(M/BIM); (b,d)LSV curves of UT-N-C(M/BIM) and UT-N@N-C(M/BIM) before and after i-t operation.

## Supplementary Tables

Table S1. XPS element content of MOFs-derived carbon (at.%)

| | C | N | O | Zn |
|---|---|---|---|---|
| N-C(BIM) | 73.2 | 12.16 | 11.86 | 2.78 |
| N-C(M/BIM) | 80.22 | 10.69 | 6.95 | 2.5 |
| UT-N-C(M/BIM) | 85.14 | 6.82 | 7.68 | 0.36 |
| UT-N@N-C(M/BIM) | 87.52 | 6.71 | 5.62 | 0.15 |

Table S2. Different N content of MOFs-derived carbon (%)

| | $N_1$ | $N_2$ | $N_3$ | $N_4$ | $N_5$ |
|---|---|---|---|---|---|
| N-C(BIM) | 37 | 26 | 11 | 7 | 19 |
| N-C(M/BIM) | 51 | 9 | 19 | 11 | 10 |
| UT-N-C(M/BIM) | 30 | 15 | 13 | 39 | 3 |
| UT-N@N-C(M/BIM) | 33 | 10 | 18 | 34 | 5 |

Table S3. ORR performance of previous reports and this work

| Catalysts | $E_{onset}$ (V) | $E_{1/2}$ (V) | Ref. |
|---|---|---|---|
| UT-N@N-C(M/BIM) | 0.98 | 0.89 | - |
| LTHT-FeP | 0.92 | 0.83 | [1] |
| NFLGDY-900c | 0.97 | 0.87 | [2] |
| AgClNW-0 | 1.01 | 0.82 | [3] |
| Fe-N-AC-1000 | 0.96 | 0.89 | [4] |

## Reference


[1] N. Zion, D. A. Cullen, P. Zelenay and L. Elbaz, *Angewandte Chemie*, 2020, **132**, 2504-251

[2] W. Sun and S. X. Dou, *Chem*, 2018, **4**, 2024-2026.

[3] S.-j. Kim, S.-C. Lee, C. Lee, M. H. Kim and Y. Lee, *Nano Energy*, 2018, **48**, 134-143.

[4] F. Zhang, D. Zhang, W. Liu, X. Li and Q. Chen, *Carbon*, 2022, **187**, 67-77